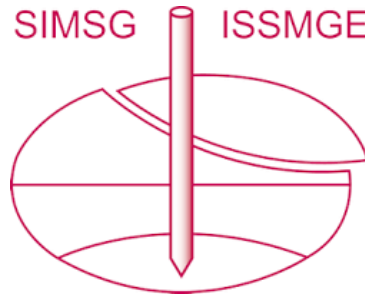


INTERNATIONAL SOCIETY FOR SOIL MECHANICS AND GEOTECHNICAL ENGINEERING



This paper was downloaded from the Online Library of the International Society for Soil Mechanics and Geotechnical Engineering (ISSMGE). The library is available here:

<https://www.issmge.org/publications/online-library>

This is an open-access database that archives thousands of papers published under the Auspices of the ISSMGE and maintained by the Innovation and Development Committee of ISSMGE.

The paper was published in the proceedings of the 10th European Conference on Numerical Methods in Geotechnical Engineering and was edited by Lidija Zdravkovic, Stavroula Kontoe, Aikaterini Tsiampousi and David Taborda. The conference was held from June 26th to June 28th 2023 at the Imperial College London, United Kingdom.

To see the complete list of papers in the proceedings visit the link below:

<https://issmge.org/files/NUMGE2023-Preface.pdf>

Replication of fall cone test on marine clay with a Generalized Interpolation Material Point Method simulation

D. Mohapatra¹, Z. Li¹, M. Saresma², J. Virtasalo², W. Solowski¹

¹*Department of Civil Engineering, Aalto University, Espoo, Finland*

²*Geological Survey of Finland, Espoo, Finland*

ABSTRACT: The paper shows a numerical simulation of a fall cone test done on a soft and sensitive marine clay sample collected from the Gulf of Finland in the Baltic Sea. The simulation involves large deformations and takes into account the destructuration of clay, strain rate effects, and non-linear material behaviour. First, the analysed fall cone test was captured with a high-speed camera (1000 frames/sec). MATLAB image processing tools helped to quantify the cone displacement, velocity, and acceleration during the indentation process. Further, we simulate the process of indentation of the cone into the soils using the Generalized Interpolation Material Point Method (GIMP). In the simulation, the undrained shear strength of soil (s_u) is taken as a function of strain rate to consider the effect of strain rate on cone indentation, as well as a function of destructuration. The presented numerical simulation replicates well the shown experiment. The simulation results indicate that the present material framework, along with GIMP, can be used to simulate the dynamic penetration process on soft and sensitive clay.

Keywords: Generalized interpolation material point method; Fall cone test; clay destructuration; strain rate effects

1 INTRODUCTION

Dynamic penetration is commonly encountered in many practical geotechnical engineering problems, such as pile driving, as well as in laboratory and in-situ soil tests. The numerical simulation of the dynamic penetration of a rigid body into the soil is a challenging problem due to large deformations and strains, the evolution of shear bands, material nonlinearity, and strain softening (e.g., Lu et al., 2001).

The Generalized Interpolation Material Point Method (GIMP) has been successfully used to study different penetration problems, such as the penetration of strip footing (Solowski & Sloan, 2015), modelling of pile installation (Phuong et al., 2016), and cone penetration tests (Ceccato et al., 2016). The above studies ignore the effects of strain rate and destructuration on the shear strength of soil during the penetration process. However, the dynamic penetration processes are associated with a wide range of strain rates. So, not considering the influence of the strain rate on the undrained shear strength of clay could have a considerable impact on numerical simulation. Furthermore, many clays are sensitive, with the undrained shear strength reducing during the indentation process due to the destructuration of clay. Not considering the effects of strain rate and destructuration on clay will significantly influence the accuracy of the numerical simulation.

This paper shows the numerical simulations of free-fall cone tests on soft and sensitive marine clay by using GIMP combined with an extended Tresca material model to consider the effects of strain rate and destructuration of clay. The displacement, velocity, and acceleration profiles associated with the cone indentation process of the fall cone experiment are obtained by using MATLAB image processing tools. The numerical simulation results that take into account the effect of strain rate and clay destructuration match the experimental observations very well.

2 FALL CONE TEST

The fall cone test is commonly used for the rapid determination of the undrained shear strength (s_u) of cohesive soil. In this test, a metal cone of weight Q (g) is positioned so that its tip touches the surface of the soil sample and is then released to fall freely under its own weight. Assuming that the final penetration depth of the cone into the soil is d_p (mm), the undrained shear strength of the soil sample is (Koumoto & Houlsby, 2015):

$$s_u = \frac{KQ}{d_p^2} \quad (1)$$

where K is the cone factor, which depends, among others, on the type and roughness of the cone and strain rate parameters.

3 EXPERIMENTAL INVESTIGATION OF CONE PENETRATION MECHANISM

In the present study, marine clay samples were collected from the Gulf of Finland in the Baltic Sea using PVC sampling tubes. The clay specimens for the fall cone tests are of approximately 40 mm thickness and were extruded from the sampling tube and then cut with a wire saw. The cylindrical specimen is directly placed in the basement of the fall cone apparatus, and the fall cone test with a 30° 100g cone is carried out at 3 different points on the sample surface (labelled Experiment 1, Experiment 2, and Experiment 3). The tests yielded final penetration depths (d_p) of 15.4mm, 16.5mm, and 16.2mm for the three associated points. The representative average value of the penetration depth (d_p) is 16.03 mm. The contact between the cone and soil is assumed to be rough, which corresponds to the cone factor $K= 1.03$ (Koumoto & Houlsby, 2001). Equation (1) indicates that the measured average penetration depth corresponds to the theoretical value of the undrained shear strength (s_u) of soil of 3.92 kPa.

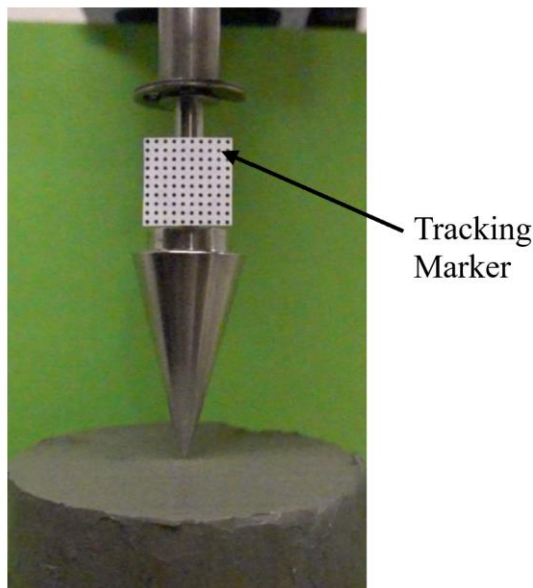


Figure 1. The 30°, 100 gm cone set up used in the experiment to track the cone.

The present study used a non-contact tracking method involving high-speed photography and subsequent image analysis to track the cone displacement throughout the fall cone experiment without influencing the motion of the cone. A high-speed camera (1000 frames/sec) recorded the whole process of the fall cone test. A white paper featuring a grid of black tracking markers attached to the cone as

shown in Figure 1 for more precise tracking. The experiment used different light and background colour combinations (shown in Figure 1) to avoid reflections and reduce noise. The digital images recorded by the camera contain brightness data recorded at each pixel point. The present study used MATLAB image processing codes based on the Kanade-Lucas-Tomasi (KLT) feature-tracking algorithm (Lucas & Kanade, 1981; Shi & Tomasi, 1994) to track the tracking markers on the cone and obtain the displacement-time profile of each tracking marker. Using an appropriate scaling factor, the displacement-time profiles produced from the image analysis in image space coordinates (pixels) are transformed to object space coordinates (meters). The velocity-time profiles associated with the tracking markers are obtained by numerically differentiating the displacement-time profiles using the central difference method. Figure (2) shows that the velocity-time profile associated with the individual tracking markers is noisy. The noise in the velocity-time curve may be due to the error induced by the use of numerical differentiation or due to the error associated with the displacement estimation. The smoothed velocity curve (shown in black) is obtained by taking the average velocity of 100 tracking points. The smoothed velocity profile is further differentiated numerically to obtain the acceleration-time profile of the cone.

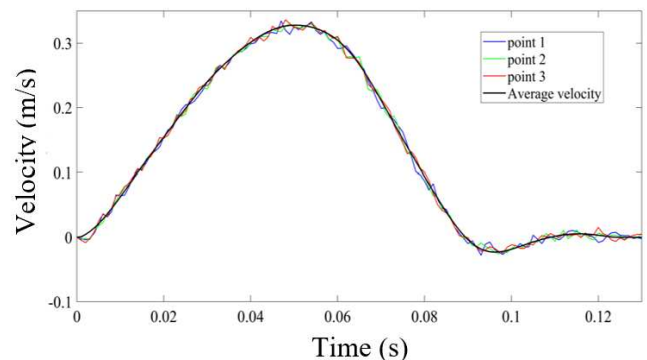


Figure 2. Velocity profiles of different tracking markers on the cone during the cone penetration process.

Table 1. Final penetration depth of cone (d_p) from different experiments

	d_p , mm (Experiment)	d_p , mm (image processing)
Experiment 1	15.4	15.5
Experiment 2	16.5	16.5
Experiment 3	16.2	16.3

The above-mentioned image processing technique is used to obtain the displacement, velocity, and acceleration profiles associated with the three experiments. Table 1 shows that the final penetration depth, obtained with the image processing technique, matches well with that obtained from the experiments. Figures 7-9 show that the displacement, velocity, and

acceleration profiles associated with different points in experiments are similar. In all cases, the penetration process takes less than 0.1 sec. The acceleration profiles in Figure 5 show that the acceleration at the very beginning of the experiment was lower than the gravitational acceleration. This slowdown may be caused by friction mobilized in the cone shaft during the cone release for free fall.

4 NUMERICAL MODELLING USING GIMP

4.1 The generalized interpolation material point method (GIMP)

The material point method (MPM) is a particle-based method well-suited to solve dynamic large deformation problems where the conventional mesh-based methods fail due to large mesh distortion (Sulsky et al., 1995). However, the original MPM has lots of numerical instability. The generalized material point method (GIMP) is an updated version of the material point method that uses a particle characteristics function to reduce cell-crossing errors (Bardenhagen & Kober, 1970). This paper uses GIMP as encoded in Uintah software (<http://uintah.utah.edu/>) for simulations of the fall cone test.

4.2 The constitutive model

The entire process of cone penetration in the fall cone test is very short (less than 0.1 sec). Therefore, for fully saturated clay, there will be no volume change (undrained conditions). Hence, the shear strength will be related to the undrained shear strength. Among others, (Boukpeti et al., 2012; Einav & Randolph, 2006; Jeong et al., 2009) show that the undrained shear strength of clay depends on the shear strain rate and deconstruction of clay. The undrained shear strength of clay under a higher shearing rate is higher than the shear strength of the same clay under a low shearing rate. Similarly, the sensitive clays show shear strength degradation with the increase in accumulated plastic strains. Therefore, in the simulations, we use the Tresca material model extended to consider the effect of strain rate and deconstruction on undrained shear strength as mentioned in (Einav & Randolph, 2006; Tran & Sołowski, 2019). The undrained shear strength of clay is expressed as a function of strain rate ($\delta\gamma$), accumulated shear strain (ξ), and sensitivity (S_t) as:

$$s_u(\delta\gamma, \xi, S_t) = s_{u,ref} \left(\frac{\delta\gamma}{\delta\gamma_{ref}} \right)^\beta \left[\frac{1}{S_t} + \left(1 - \frac{1}{S_t} \right) e^{\frac{-3\xi}{\xi_{95}}} \right] \quad (2)$$

where $s_{u,ref}$ is reference shear strain at reference strain rate ($\delta\gamma_{ref}$), β is the strain rate parameter associated with the power law, and ξ_{95} is the accumulated shear strains required to obtain 95% reduction of the shear

strength. For small deformations, the dynamic undrained shear modulus depends on the shear strain rate, therefore the dynamic undrained shear modulus can be estimated as

$$G_u(\delta\gamma) = G_{u,ref} \left(\frac{\delta\gamma}{\delta\gamma_{ref}} \right)^\beta \quad (3)$$

4.3 Numerical Modelling of fall-cone test

The GIMP simulation of the fall cone test replicates the experiment using an axisymmetric assumption to reduce the computational cost associated with the 3D MPM simulation. Figure 3 shows the numerical model and associated boundary conditions. The GIMP simulation uses the rigid material model to model the steel cone with 100g weight and 30° cone angle. The Tresca material model, with the cohesion dependent on the strain rates and sensitivity (as mentioned in Equations (2) and (3)) is used to model the marine clay. The measured value of sensitivity of the clay (S_t) sample is 10. As mentioned in Section (2), the value of reference undrained shear strength ($s_{u,ref}$) is 3.92 kPa based on the theoretical solution of (Koumoto & Houlsby, 2015) for rough cone-soil interface conditions. The range of strain rate in a fall cone test is roughly the same as in a vane shear test. The value of the reference shear strain is set to 0.5 s^{-1} based on the vane shear data of (Boukpeti et al., 2012). The value of β is set to be 0.06, which is the reasonable average of the values of β reported in different literature (Chung et al., 2006; Rattley et al., 2008). The reference elastic shear modulus is set to be 167 times the undrained reference shear strength value as indicated by (Moavenian et al., 2016). Table (2) summarizes the various model parameters considered in the study.

Table 2. Material parameters for numerical simulation

$s_{u,ref}$ (kPa)	$\delta\gamma_{ref}$ (s^{-1})	β	$G_{u,ref}$ (kPa)	ν_u	S_t	ξ_{95}
3.95	0.5	0.06	$167s_{u,ref}$	0.499	10	25

The simulations assume frictional contact with friction coefficient (μ) developed by Bardenhagen et al. (2001). The friction coefficient between cohesive soil and steel lies between 0.5-0.65 (Tsubakihara et al., 1993). A series of numerical studies have been conducted to examine the influence of the friction coefficient on cone penetration depth by varying the friction coefficient (μ) from 0 to 1. Figure (4) demonstrates that friction coefficients, greater than 0.6, do not significantly change the penetration depth. This shows that the friction coefficient ($\mu = 0.6$) is enough to prevent sliding between the cone and the soil. Therefore, in the present analysis, we selected the friction coefficient $\mu = 0.6$.

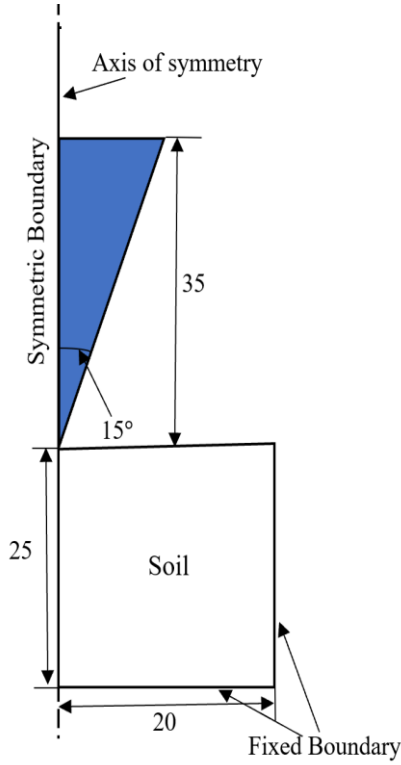


Figure 3. Schematic of a fall-cone test. Unit: mm

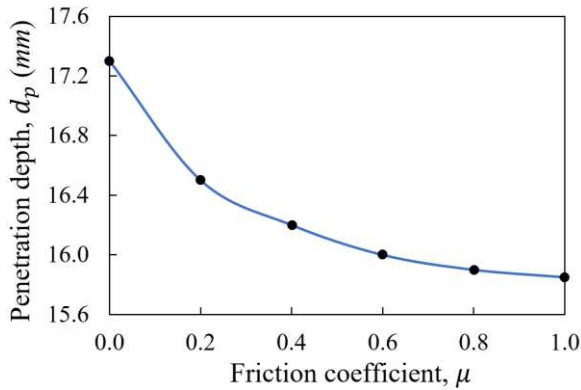


Figure 4. Influence of friction coefficient on the penetration depth of the cone

5 GIMP SIMULATION RESULTS

5.1 Numerical error due to grid density

The grid density in GIMP plays a crucial role in the accurate simulation of the fall cone test (Tran et al., 2017). To investigate how the grid density impacts the simulation results, the analysis discretizes the problem domain in Figure (1) by using a structured mesh of square sizes ($h \times h$) where $h = 1, 0.5, 0.25,$ and 0.125 mm, each time with 4 material points in the cell. These correspond to 4960, 19840, 79360, and 317440 material points in the simulation, respectively. For a given value of undrained shear strength, the theoretical penetration depth ($d_{p,theo}$) computed theoretically using Equation (1) and the numerical value of penetration depth

($d_{p,num}$) is obtained from the numerical simulation. The error associated with the fall cone analysis is defined as:

$$\text{error} = \frac{d_{p,theo} - d_{p,num}}{d_{p,theo}} \% \quad (4)$$

Figure (5) demonstrates that when the number of grid cells increases, the error decreases. For a given mesh density, the error associated with a higher penetration depth is smaller than that associated with a lower penetration depth. That may be because there are fewer material points in the area of penetration. Additionally, Figure (5) shows that the error associated with $h = 0.125$ mm is less than 5% in all the cases, and for $d_{p,theo} = 16$ mm, the value of the numerical penetration depth is almost the same as the theoretical penetration depth. Therefore, the present analysis uses $h = 0.125$ mm to simulate the fall cone test numerically. Figure (5) also confirms that the theoretical value of undrained shear strength obtained by using Equation (1) can be used for further simulation of the fall cone test.

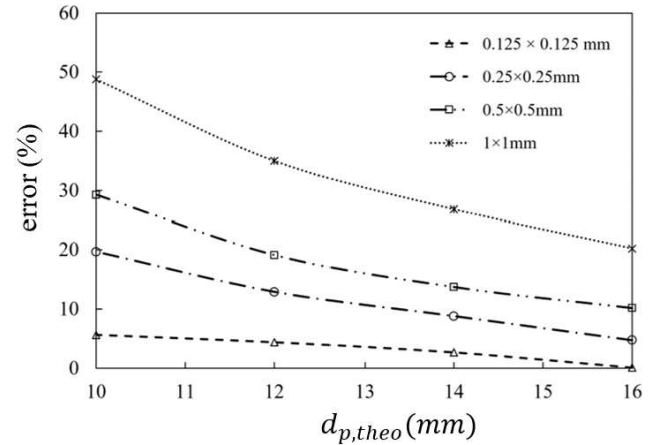


Figure 5. Spatial discretisation errors of numerical solution

5.2 Numerical replication of fall-cone tests

The numerical simulation uses grid size $h = 0.125$ mm and material parameters as given in Table 1 for $\mu = 0.6$. Figure 9 shows that the cone takes around 0.01s of time from the beginning to reach the free-fall condition. This is taken into consideration in the numerical simulation by increasing the acceleration due to gravity linearly from 0 to 0.01s. After 0.01s, the acceleration due to gravity is fixed to a constant value (9.819 m/s^2). In this way, the weight of the clay at the very beginning of the simulation (0 to 0.01s) will not accurately represent the actual weight of the clay. To examine the impact of the inaccurate weight of clay on displacement at the beginning of the simulation (0 to 0.01s), the numerical simulations of the fall cone test are carried out for different unit weights of the soil by keeping all other parameters unchanged and the simulated cone

displacements are presented in Figure (6). Figure (6) shows that the inaccurate value of the unit weight of soil does not significantly impact the numerical simulation results, as the displacement of the soil in the first 0.01s is minimal. Furthermore, the soil weight affects the overall results only marginally, as the majority of the initial potential energy of the cone is dissipated via plastic work during shearing.

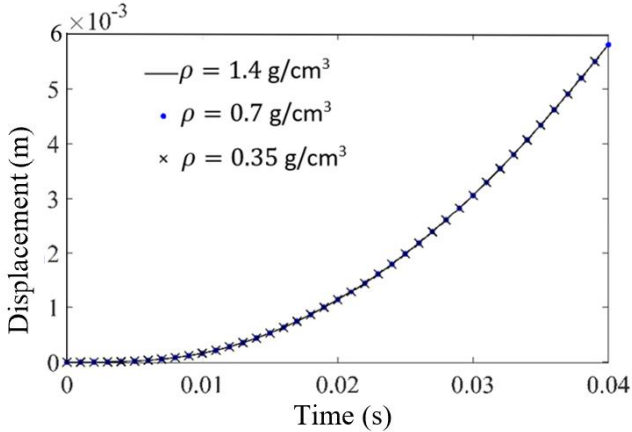


Figure 6. Cone displacements simulated with three different soil unit weight assumptions (all the other parameters constant)

Figures 7, 8, and 9 compare the development of penetration depth, velocity, and acceleration over time between the experiments and the numerical simulation. Figures 7-9 demonstrate that the numerical and experimental profiles of displacement, velocity, and acceleration associated with the cone penetration process match quite well. In the experiments, the cone reached its final penetration depth in roughly 0.1s, whereas in the numerical simulation it took around 0.09s. The final penetration depth obtained from the numerical simulation (15.99 mm) is close to the average penetration depth obtained from the experiments (16.03 mm). Figure 7 also shows that the cone rebounded around 0.25mm in Experiment 2 and Experiment 3, while Experiment 1 did not show any rebound. The numerical simulation shows a rebound of approximately 0.2mm. Figure 8 demonstrates that the numerical model predicts the maximum velocity to be approximately 0.33 m/s, which is close to the average maximum velocity from the experiment (0.31 m/s). Figure 9 shows that the numerical cone acceleration oscillates at the completion of the penetration process, with the amplitude of these oscillations decreasing gradually over time. As GIMP is a completely explicit approach that takes into account dynamic forces, the oscillations are presumably the result of the assumed elastic behaviour of the material in the Tresca model at stresses below yield.

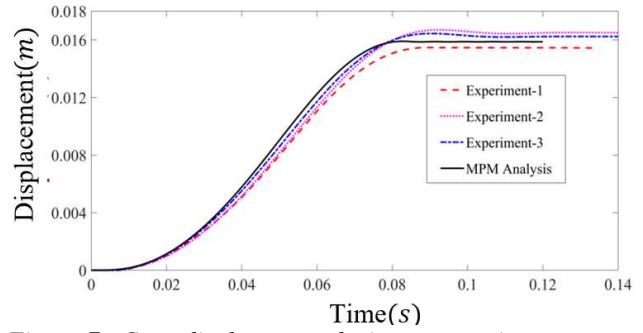


Figure 7. Cone displacement during penetration

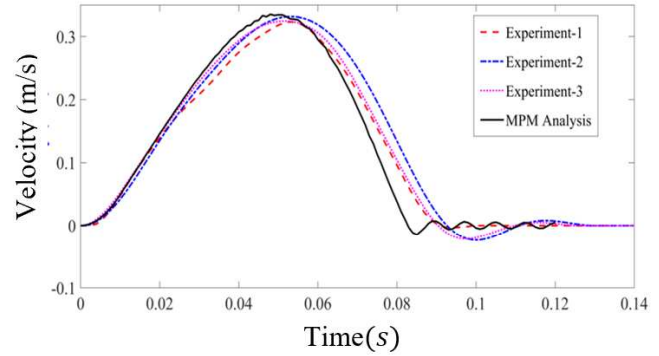


Figure 8. Cone velocity during penetration

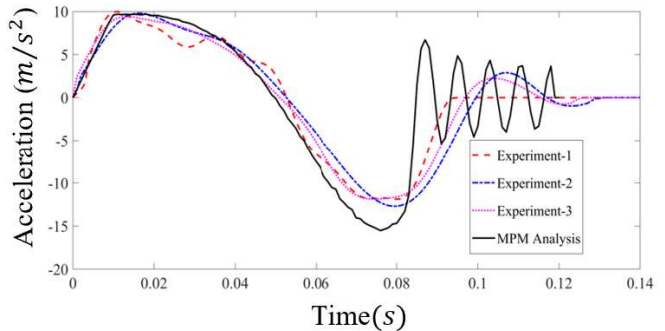


Figure 9. Cone acceleration during penetration

6 CONCLUSIONS

The fall cone test is frequently used to measure the undrained shear strength of soil. The interpretation of the undrained shear strength of soil based on the fall cone test is rather challenging since it is dependent on various factors such as the cone angle, the roughness of the cone, the strain rate parameters related to cone penetration, and so on. In this study, the fall cone experiment is carried out on soft and sensitive marine clay samples collected from the Gulf of Finland in the Baltic Sea. The displacement, velocity, and acceleration profiles associated with the cone indentation process in the fall cone experiment are obtained by using MATLAB image processing tools. The numerical simulation using the Generalized Material Point Method (GIMP) combined with the Tresca material model extended to consider the effect of strain rate and

strain softening due to the destructuration of clay shows a good agreement with both theoretical and experimental results. The experimental results are very well replicated by the numerical simulation, with an excellent agreement not only of the final depth of the penetration but also of the displacement, velocity, and acceleration profiles during the penetration. The results show that with the right strain rate and sensitivity, the dynamic penetration parameters and high grid density, GIMP simulations can replicate the mechanisms relevant to the penetration of cone into clay. The study also suggests that the strain rate and destructuration of clay greatly affects the kinematic behaviour of the cone.

7 ACKNOWLEDGEMENTS

This research is part of the Geomeasure project, funded by the Academy of Finland (grant number 347602).

8 REFERENCES

- Bardenhagen, S. G., Guilkey, J. E., Roessig, K. M., Brackbill, J. U., Witzel, W. M., & Foster, J. C. (2001). An Improved Contact Algorithm for the Material Point Method and Application to Stress Propagation in Granular Material. *CMES*, 2(4), 509–522.
- Bardenhagen, S. G., & Kober, E. M. (1970). The Generalized Interpolation Material Point Method. *Computer Modeling in Engineering & Sciences*, 5(6), 477–496.
- Boukpeti, N., White, D. J., Randolph, M. F., & Low, H. E. (2012). Strength of fine-grained soils at the solid-fluid transition. *Geotechnique*, 62(3), 213–226.
- Ceccato, F., Beuth, L., Vermeer, P. A., & Simonini, P. (2016). Two-phase Material Point Method applied to the study of cone penetration. *Computers and Geotechnics*, 80, 440–452.
- Chung, S. F., Randolph, M. F., & Schneider, J. A. (2006). Effect of Penetration Rate on Penetrometer Resistance in Clay. *Journal of Geotechnical and Geoenvironmental Engineering*, 132(9), 1188–1196.
- Einav, I., & Randolph, M. (2006). Effect of strain rate on mobilised strength and thickness of curved shear bands. *Geotechnique*, 56(7), 501–504.
- Jeong, S. W., Leroueil, S., & Locat, J. (2009). Applicability of power law for describing the rheology of soils of different origins and characteristics. *Canadian Geotechnical Journal*, 46(9), 1011–1023.
- Koumoto, T., & Houlsby, G. T. (2015). Theory and practice of the fall cone test. *51*(8), 701–712.
- Lu, Q., Hu, Y., & Randolph, M. F. (2001). *Deep Penetration In Soft Clay With Strength Increasing With Depth*. The Eleventh International Offshore and Polar Engineering Conference, Stavanger, Norway.
- Lucas, B. D., & Kanade, T. (1981). An iterative image registration technique with an application to stereo vision. *Proceedings of the 7th International Joint Conference on Artificial Intelligence*, 674–679.
- Moavenian, M. H., Nazem, M., Carter, J. P., & Randolph, M. F. (2016). Numerical analysis of penetrometers free-falling into soil with shear strength increasing linearly with depth. *Computers and Geotechnics*, 72, 57–66.
- Phuong, N. T. V., van Tol, A. F., Elkadi, A. S. K., & Rohe, A. (2016). Numerical investigation of pile installation effects in sand using material point method. *Computers and Geotechnics*, 73, 58–71.
- Rattley, M. J., Richards, D. J., & Lehane, B. M. (2008). Uplift Performance of Transmission Tower Foundations Embedded in Clay. *Journal of Geotechnical and Geoenvironmental Engineering*, 134(4), 531–540.
- Shi, J., & Tomasi, C. (1994). Good features to track. *Proceedings of the IEEE Computer Society Conference on Computer Vision and Pattern Recognition*, 593–600.
- Solowski, W. T., & Sloan, S. W. (2015). Evaluation of material point method for use in geotechnics. *International Journal for Numerical and Analytical Methods in Geomechanics*, 39(7), 685–701.
- Sulsky, D., Zhou, S. J., & Schreyer, H. L. (1995). Application of a particle-in-cell method to solid mechanics. *Computer Physics Communications*, 87(1–2), 236–252.
- Tran, Q. A., & Sołowski, W. (2019). Generalized Interpolation Material Point Method modelling of large deformation problems including strain-rate effects - Application to penetration and progressive failure problems. *Computers and Geotechnics*, 106, 249–265.
- Tran, Q. A., Solowski, W., Karstunen, M., & Korkiala-Tanttu, L. (2017). Modelling of Fall-cone Tests with Strain-rate Effects. *Procedia Engineering*, 175, 293–301.
- Tsubakihara, Y., Kishida, H., & Nishiyama, T. (1993). Friction between Cohesive Soils and Steel. *Soils and Foundations*, 33(2), 145–156.